Genetic relationship between shell fossils and shale oil: A case study of Jurassic shale reservoir in the northeast Sichuan Basin

Yong Ma, Cheng–yu Yang, Da–hua Li, Hong–wei Zhao, Zhe–jun Pan, Yong–shui Zhou, Dai–duo Zhu, Ning–ning Zhong

---

Related articles that may interest you

Mesozoic–Cenozoic stress field magnitude in Sichuan Basin, China and its adjacent areas and the implication on shale gas reservoir: Determination by acoustic emission in rocks
China Geology. 2020, 3(4), 591 https://doi.org/10.31035/cg2020068

Formation, evolution, reconstruction of black shales and their influence on shale oil and gas resource
China Geology. 2024, 7(3), 551 https://doi.org/10.31035/cg2024060

Pacific oyster (*Crassostrea gigas*) shell growth duration in a year in Bohai Bay and implication for its carbon sink potential
China Geology. 2024, 7(4), 653 https://doi.org/10.31035/cg2023054

Coupling relationship between reservoir diagenesis and hydrocarbon accumulation in Lower Cretaceous Yingcheng Formation of Dongling, Changling fault depression, Songliao Basin, Northeast China
China Geology. 2020, 3(2), 247 https://doi.org/10.31035/cg2020004

Geological characteristics of unconventional tight oil reservoir (10^9 t): A case study of Upper Cretaceous Qingshankou Formation, northern Songliao Basin, NE China
China Geology. 2024, 7(1), 51 https://doi.org/10.31035/cg2022072

Distribution characteristics, exploration and development, geological theories research progress and exploration directions of shale gas in China
China Geology. 2022, 5(1), 110 https://doi.org/10.31035/cg2021069

China Geology

Genetic relationship between shell fossils and shale oil: A case study of Jurassic shale reservoir in the northeast Sichuan Basin

Yong Ma[a,*], Cheng-yu Yang[a], Da-hua Li[b], Hong-wei Zhao[c], Zhe-jun Pan[d], Yong-shui Zhou[e], Dai-duo Zhu[a], Ning-ning Zhong[a]

[a] *State Key Laboratory of Petroleum Resources and Engineering, China University of Petroleum (Beijing), Beijing 102200, China*

[b] *Key Laboratory of Shale Gas Exploration (Chongqing Institute of Geology & Mineral Resource), Ministry of Natural Resources, Chongqing 401120, China*

[c] *Exploration Department of PetroChina, Daqing Oilfield Co Ltd, Daqing, Heilongjiang 163453, China*

[d] *State Key Laboratory of Continental Shale Oil, Northeast Petroleum University, Daqing, Heilongjiang 163318, China*

[e] *Zhongyuan Oilfield Company, SINOPEC, Puyang 457001, China*

A R T I C L E   I N F O

A B S T R A C T

Benthic bivalves, the most widely distributed mollusks since the Mesozoic era, often inhabited environments where their fossilized remains are found adjacent to or intermingled with organic-rich shale. Recent Jurassic shale oil exploration in the Sichuan Basin has revealed that bioclastic layers, composed of abundant fossil bivalves and closely associated with shales and, exhibit significant hydrocarbon potentials. However, the microscopic structures of these bivalve fossils and their role in hydrocarbon storage and migration remain poorly understood. In this study, we characterized the microporosity of bivalve shells within the Middle-Lower Jurassic bioclastic shale in the northeastern Sichuan Basin using a combination of 2D imaging (thin section, SEM), 3D reconstruction (FIB-SEM), and permeability simulation. The micropores within the shell fossils range from 100 to 1000 nm in radius and are uniformly distributed in a grid-like pattern within the shell interior, where they host liquid hydrocarbons. The bioclastic carbonate layers exhibit an overall porosity of approximately 0.8%. Comparative analysis with extant bivalve shells suggests that these micropores represent residual pores from the nacreous brick wall structure. Due to the regular orientation of the shells and their microporous nacres, permeability coefficients along the long bivalve fossil axes are three to five times higher than those along the short axes. These residual micropores within the bioclastic fossil shells have a positive influence on both the storage and migration of shale oil and gas, making bioclastic fossil-bearing shalespromising sweet spots for shale oil and gas exploration in similar sedimentary environments.

©2025 China Geology Editorial Office.

1. Introduction

Shale oil and shale gas refer to petroleum and natural gas accumulations primarily found in organic-rich shales. Petroleum compounds exist in an adsorbed state on mineral surfaces, adsorbed or absorbed in kerogen or as a free phase within the fractures and pore systems of shale (Jarvie DM, 2012; Pepper A et al., 2019; Romero-Sarmiento MF, 2019; Ma Y et al., 2020). Broadly, the definition of shale oil and gas can be extended to natural hydrocarbon accumulations found in siltstone, argillaceous siltstone, and even sandstone interlayers within carbonaceous shale formations that exhibit typical self-generation and self-storage characteristics (Loucks RG et al., 2012; Raji M et al., 2015; Horsfield B et al., 2020). Since the early 21st century, the commercial development of shale oil and gas in the United States has achieved tremendous success due to the increasing maturity of horizontal drilling and staged fracturing technologies (Curtis JB, 2002; Ghanizadeh A et al., 2020). In contrast to shale oil formations deposited in marine sedimentary environments in the United States, shale oil systems in China predominantly formed in terrestrial lacustrine environments. In contrast to the extensive and continuous distribution of marine sedimentary rocks, lacustrine strata exhibit significant variability in vertical and horizontal directions, resulting in complex lithological and geochemical heterogeneity, thereby

---

posing greater challenges for shale oil exploration (Katz B and Lin F, 2014; Ji WM et al., 2024).

China is home to extensive and continuously distributed terrestrial shale formations, many of which exhibit favorable conditions for shale oil formation due to their characteristics such as significant single-layer thickness, high organic carbon content, moderate thermal evolution, high brittle mineral content, and good oil-bearing capacity (Wang XN et al., 2022; Jin ZJ et al., 2023; Yuan SY et al., 2023). These shale formations, characterized by abundant resources, present promising prospects for exploration and development. Significant breakthroughs in terrestrial shale oil and gas exploration have been made in various basins, including the Songliao Basin, Bohai Bay Basin, Ordos Basin, and Sichuan Basin, with the main shale facies including clayey shale, shell (intermittent) lamina-thin-layered clayey shale facies, (laminated) silty shale facies, clayey shell calcareous shale facies, silty clayey shale facies, and shell calcareous silty shale facies. (Wang XN et al., 2022; Cao YC et al., 2023; Jin ZJ et al., 2023). Among them, the organic-rich shales of the Middle-Lower Jurassic in the northeastern Sichuan Basin, distinguished by high abundance of organic matter, high maturity, and relatively high brittleness, are considered exceptional terrestrial shale oil and gas reservoirs (Yang YM et al., 2019; Liu ZB et al., 2020; He WY et al., 2022). These Jurassic organic-rich shales frequently contain numerous layers or interlayers of biogenic shells, and recent studies suggest that these shells may play a significant role in the storage and migration of oil and gas (Ni C et al., 2012; Zhu HH et al., 2022).

Bivalve mollusks, classic benthic creatures, typically attach themselves to sandy or muddy substrates at the aquatic depths, demonstrating slow and limited mobility (Rindsberg AK, 1994; Uchman A et al., 2011). Their primary mechanism for nutrient acquisition involves ingesting sediment from the substrate, filtering out organic matter within, or directly preying on organic detritus and microscopic aquatic organisms (Bender K and Davis WR, 1984; Mangano MG et al., 1998). The Bivalvia class, a member of the mollusk family, is distinguished by its shell, primarily consisting of carbonate minerals and displays a remarkable diversity of species (Addadi L et al., 2006). The majority of these species inhabit the marine environments, while a few thrive in freshwater ecosystems (Huang YF et al., 2015). Following to the catastrophic Permian-Triassic extinction event, bivalves gradually become the dominant benthic organisms globally, a position they continue to hold until the present day (Huang YF et al., 2015).

Bioclastic shale, a common rock type in unconventional reservoirs, is frequently located adjacent to fine-grained sediments, such as shale, and exhibits superior physical properties and brittleness (Ni C et al., 2012; Zhu HH et al., 2022). Its oil-bearing properties have attracted increasing attention in the search for unconventional oil and gas resources (Zhu HH et al., 2022). Horizontal microfractures form between shell fossils and micropores within the shells

constitute the primary reservoir spaces in bioclastic shale (Zhu HH et al., 2022). Micropores within the shells have been identified as key hydrocarbon-enrichment areas within this rock type (Zhu HH et al., 2022). However, there is a significant gap of understanding regarding the characteristics, origin, and petroleum geological implications of these pores. This paper examines the genesis, characteristics, and hydrocarbon storage and migration potential of micropores in bioclastic shale, using representative samples from the Lower Jurassic strata in the northeastern Sichuan region. Using multi-scale micro-analysis methods and fluorescence microscopy, this study provides new insights into the exploration and development of unconventional oil and gas resources in this rock type.

2. Geological setting

The Sichuan Basin, located in southwestern China, is a large geological basin that primarily composed of pre-Permian marine deposits. Starting in the Triassic period and continuing to the present day, it transitioned into terrestrial formations, with the Jurassic period marked by large-scale terrestrial lacustrine basins (Yang YM et al., 2019; Liu ZB et al., 2020; He WY et al., 2022). The research area is located in northeastern Sichuan province, focusing on the Da'anzhai section of the Ziliujing and Lianggaoshan Formations, both of which are belong to the Early to Middle Jurassic eras (Fig. 1). Previous investigations of the Early Jurassic in this region of Sichuan basin suggest that the Jurassic rocks from this period consist of characteristic terrestrial clastic sediments, dominated by delta-lacustrine facies, with a thickness spanning between 1,500 to 4,000 meters (Figs. 1a, 1c). These strata exhibit a parallel unconformity with the Upper Triassic Xujiahe Formation at the base and the Cretaceous at the top (Yang YM et al., 2019; Liu ZB et al., 2020; He WY et al., 2022). In the northeastern Sichuan region, the Jurassic strata progress from the base to the top, comprising the Lower Jurassic Ziliujing Formation and the Middle Jurassic Lianggaoshan Formation (Fig. 1). Contain of, the Da'anzhai section of the Ziliujing Formation and the middle to upper sections of the Lianggaoshan Formation contain of bioclastic shale (Fig.1). The purity and thickness of the bioclastic shale in the Da'anzhai section are significantly higher than those found in the Lianggaoshan Formation. Comprehensive lithological analyses of wells and outcrops indicate that the thickness of bioclastic shale in the Da'anzhai section ranges from approximately 15 to 80 meters, constituting 60 to 80 percent of the total thickness of this layer. In contrast, the Lianggaoshan Formation contains 5 to 30 meters of bioclastic layers, representing 10 to 20 percent of its total thickness (Fig. 1).

3. Samples and methods

The samples used in this study were collected from drill cores and selected outcrops in the northeastern Sichuan region. Basic geological information for the samples is provided in Table 1. Well locations and outcrop positions are
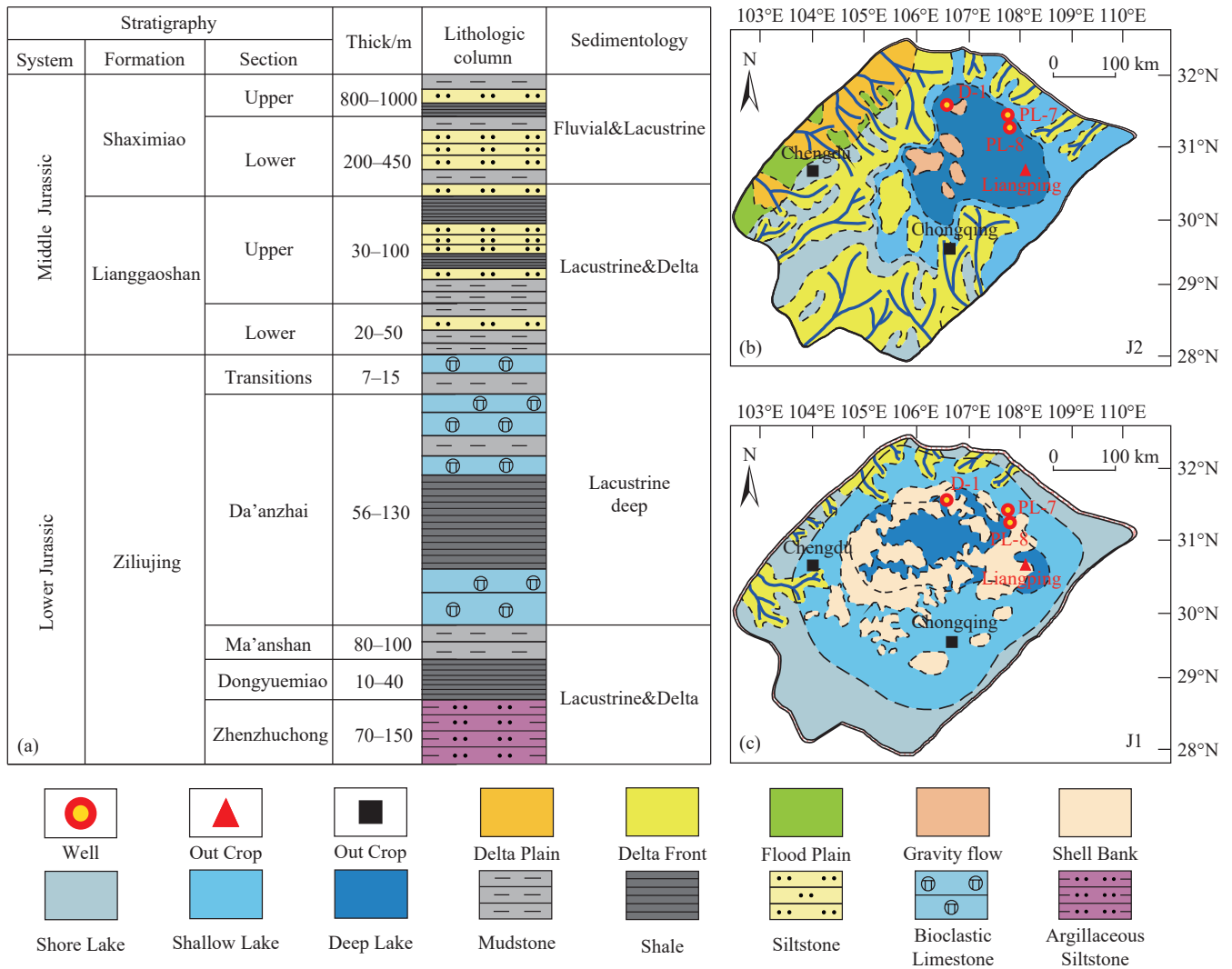
Fig. 1. Sedimentary stratigraphy and sedimentary evolution characteristics of the Jurassic Strata in the Northeastern Sichuan Basin (Modified from He WY et al., 2022). (a) Sedimentary stratigraphy of the Lower and Middle Jurassic in NE Sichuan. (b) Map of sedimentary facies of Sichuan Basin in middle Jurassic. (c) Map of sedimentary facies of Sichuan Basin in early Jurassic.

Table 1.   Basic geological information and mineral composition of the bioclastic shale samples analyzed in this study.

Well	Depth/m	Formation/Section	Mineral composition/%					
			Quartz	Feldspar	Calcite	Dolomite	Pyrite	Total Clay
PL8	2570.3	Lianggaoshan	27.1	8.6	11.6			52.7
PL8	2711	Da'anzhai	38.5	11.3	12.7			37.6
PL7	2968.3	Lianggaoshan	29.0	11.3	8.2		0.6	50.9
D1	3162.8	Lianggaoshan	33.1	3.7	42.7			20.5
D1	3363.7	Da'anzhai	10.4	4.1	83.8			1.8
D1	3364.9	Da'anzhai	35.2	12.8	23.8		2.4	25.8
D1	3368.2	Da'anzhai	30.3	7.4	21.8	10.4	1.6	28.5
D1	3371.97	Da'anzhai	16.7	1.1	54.4			27.8
D1	3376.7	Da'anzhai	36.8	12.3	8.6		2.4	40.0
Liangping	Outcrop	Da'anzhai	3.3		96.7			

depicted on the map (Figs. 1b–c). Both core and outcrop samples were sectioned and examined under a Zeiss Axio Imager 2 microscope, with employed both conventional thin sections and fluorescence thin sections.

Following Ar-ion milling, the samples were mounted on scanning electron microscope (SEM) stubs using carbon paste and coated with carbon to form a conductive surface layer.

The samples were subsequently placed into a Zeiss Crossbeam 540 focused ion beam-scanning electron microscope (FIB-SEM) for FIB milling and SEM imaging. In this system, a focused 30-kV gallium ion beam mills the samples by sputtering shale material away. The SEM captures images the freshly milled shale surface *in situ* with a resolution of 10 nm at a 2 kV accelerating voltage. The ion

and electron beams are positioned at a 54° angle relative to each other. This milling and imaging procedure was repeated 1500 times, generating a sequence of backscattered electron (BSE) images that created a 3-D dataset of the internal microstructure of the shale. The dataset was then imported into Avizo® Fire 9.3 imaging software to generate a 3-D rendering of the shale. Subsequent quantitative analysis of shell fossils were performed by assigning gray-scale values and setting thresholds to segment the features.

The Avizo software has been widely used to quantify the absolute permeability of connected pore networks in each sample by employing a finite element image-based simulation method (Peng S et al., 2014; Callow B et al., 2018; 2020). Absolute permeability, the intrinsic property of a porous medium that allows the transmission of a single-phase fluid, is direction-dependent and can be represented as a vector. In this study it will be simply referred to as "permeability". The Avizo software uses a simplified Navier-Stokes (N-S) equation to compute the single-phase laminar (low Reynolds number) volume flow of an incompressible Newtonian fluid through the pore network and to calculate the permeability tensor based on Darcy's law (Callow B et al., 2020). In this simulation, the pore fluid was assumed to be water. The fluid pressures for the pore network calculation were set to 1.3×10^5 Pa upstream and 1.0×10^5 Pa downstream in three directions.

X-ray micro computed tomography (CT) is the ideal non-destructive non-destructive method to characterize complex pore structure and mineral composition of rocks in 3D visualization (Tiwari P et al., 2013). The structures of the shales containing biological shells were analyzed using a Sanying Precision high-resolution micro-CT (Nano Voxel3502E). X-rays are generated by an electron beam with a 150kV voltage and 37.5W power and filtered through a fluorite lens 0.213 mm in diameter to reduce the beam-hardening artifact. A conical beam is projected onto a flat panel detector with a pixel matrix of 1920×1920×1536, amplifying the attenuation projection to achieve a resolution of 15 μm pixels. For micro-CT imaging, standard rock plungers with a diameter of 25mm were drilled from shale cores using a digitally controlled wire saw. The original images were imported into Avizo® Fire 9.3 imaging software for 3D reconstruction. Features were segmented by setting threshold values on gray levels, enabling the rendering of biological shells and matrix pores in the software.

4. Results

4.1. Petrology

4.1.1. Lithological assemblage

In both the Lianggaoshan Formation and the Da'anzhai section, bioclastic layers are found adjacent to fine-grained sediments such as shale and siltstone (Fig. 1). The proportion of bioclasts within the strata varies significantly, with concentrations of ranging from 50% to 90% (Figs. 2a–c). In other instances, small amounts of bioclasts are found in very thin layers interbedded within shales or fine siltstones (Yang

YM et al., 2019; Liu ZB et al., 2020; He WY et al., 2022). Various studies have shown that the lake in northeastern Sichuan Basin reached its maximum depth during the deposition of the Lower Jurassic (Yang YM et al., 2019; Liu ZB et al., 2020; He WY et al., 2022; Zhu HH et al., 2022) (Fig. 1). As a result, high-purity bioclastic and micritic layers occur in the shale of the Da'anzhai Formation. However, at the onset of the Upper Jurassic, the lake water in the research area began to shallow (Fig. 1), and pure bioclastic or micritic layers are rarely observed in the Lianggaoshan Formation. Shell layers, however, are commonly sandwiched between shales (Yang YM et al., 2019; Liu ZB et al., 2020; He WY et al., 2022).

4.1.2. Characteristics of bioclastic layers

The bioclastic intervals are consist of a granular framework formed by bioclasts and the interstitial materials surrounding them (Fig. 2). The primary interstitial materials include argillaceous, siltstone, or silty components. The bioclasts primarily consist of carbonate-rich fossil fragments, including curved surface morphology, observable in both rock samples and three-dimensional reconstructions from CT scan images (Figs 2d–e). XRD results indicate that calcite content of the bioclastic layers range from 8.2% to 96.7% (Table 1), reflecting variations in bioclast content.

Two types of shell fossils can be clearly distinguished in the thin sections: large shells and small shells (Fig. 3). The large shells appear relatively flat and thick within the rock, with thicknesses typically ranging from 0.2 to 0.5 mm in thickness (Figs. 3a–b). Their interior consists entirely of carbonate minerals, with the main body displaying fibrous aragonite pseudomorphs of calcite layers (Figs. 3a–b). The carbonate minerals at the edges exhibit a crystallization pattern distinct from that of the main body (Figs. 3a, 3e, 3h), however some shell fossils contain relatively pure calcite crystals (Figs. 3f, 3i).

The other type consists of thin shells (10-50 μm), referred to as small shells, which can occur alongside thick shells or be dispersed individually within an argillaceous and siltstone matrix (Figs. 3c–d, 3g). The interior of the thin shells is primarily composed of calcite, with aragonite pseudomorphs present (Fig. 3g). Due to their thinness, the differences in mineral crystallization between the edges and the interior are less distinct. However, thin shells generally exhibit a higher degree of curvature compared to the thick shells (Figs. 3c, 3g).

4.2. Reservoir characteristics of bioclastic layers

4.2.1. Physical properties and pore structure

Scanning electron microscope (SEM) images reveal the widespread presence of micropores within the bioclasts (Fig. 4), exhibiting significant size variations in size ranging from tens of nanometers to several micrometers (Figs. 4a–c). Some of these pores display a rectangular calcite pseudomorph feature, while others have triangular, polygonal, and other shapes (Fig. 4c). These pores are arranged in a regular
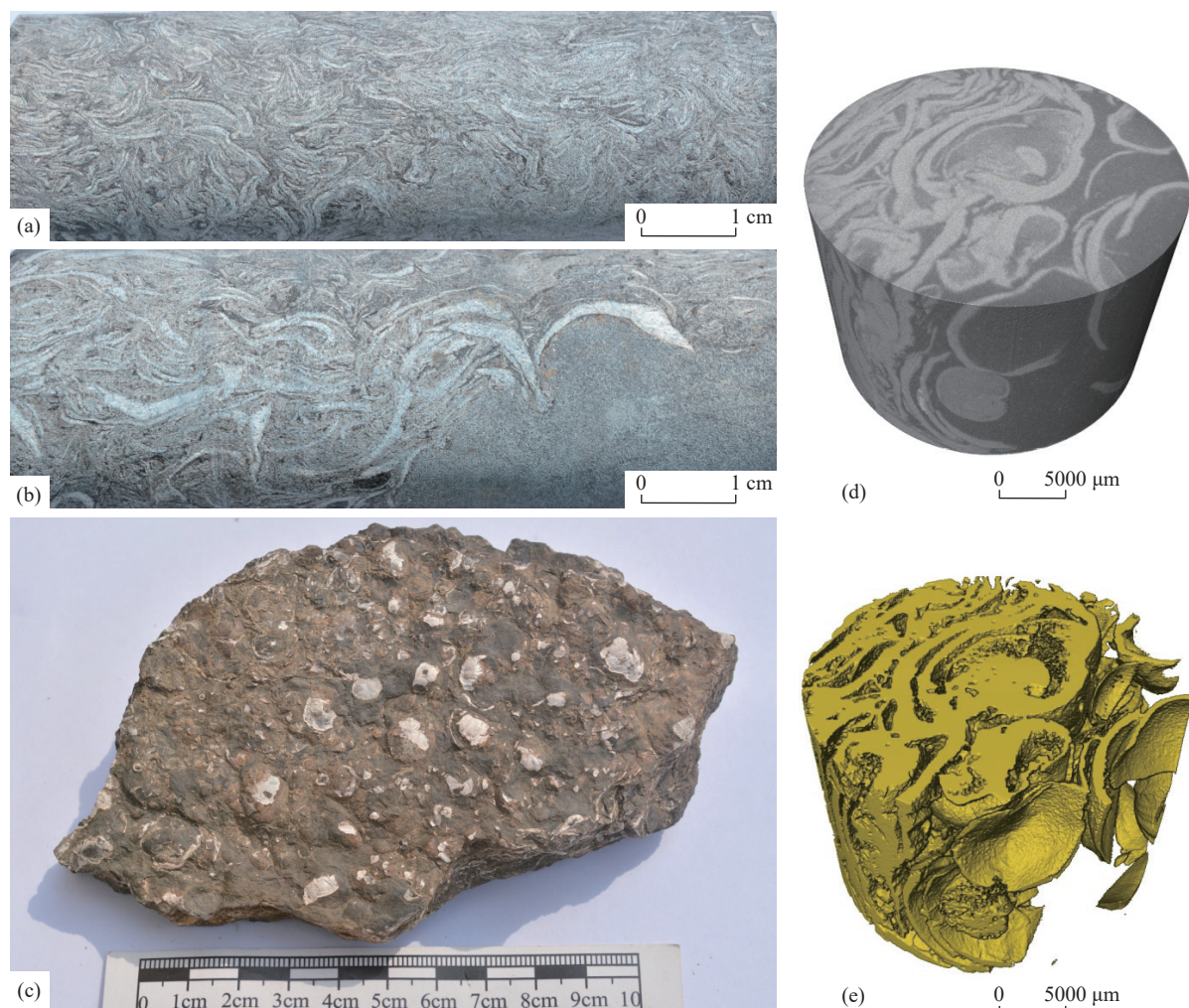
Fig. 2. Characteristics of shell fossils in bioclastic shale. (a) Pure bioclastic shale; PL8, 2711 m. (b) bioclastic shale-micrite shale; PL7, 2968.3 m. (c) Shell-rich mudstone; Outcrop, Liangping. (d) Three-dimensional reconstruction of a bioclastic shale using CT images; D1, 3162.8 m. (e) Three-dimensional reconstruction of shells within a bioclastic shale; D1, 3162.8 m.

network pattern within the shell (Figs. 4d–f). However, the pore network does not completely occupy the entire shell; rather, it forms a banded distribution along the long axis of the shell, creating a pore-rich layer (Figs. 4b, 4d–f).

Three-dimensional reconstructions of FIB-SEM images reveal that the pore distribution within the shell fossil exhibits distinct directionality, forming a lattice-like pattern in the shell's interior, though with moderate connectivity (Fig. 5). The pore radius within the shell fossil ranges from 6 to 530 nm, with the dominant pore radius spanning from 16 to 100 nm, representing typical nanometer-sized pores (Fig. 5d). Although small pores dominate numerically, the largest volumetric contribution comes from pores with a radius greater than 100 nm (Fig. 5d). The total porosity of the shell fossils calculated from the FIB-SEM reconstruction is 0.81%.

Most of the pores are arranged in planes that are obliquely oriented within the fossil shell layer (Fig. 6). As a result, fluid flow along both the x-axis and z-axis is expected to occur obliquely aligned with the extension direction of the pore planes (Figs. 6b, 6d), meanwhile fluid flow along the y-axis remains unaffected (Fig. 6c). Permeability simulations further highlight the anisotropy within the shell, showing that

computed permeability coefficients in the y-axis direction are approximately five times higher than those in the x-axis direction and three times higher than in the z-axis direction (Fig. 6; Table 2).

4.2.2. The oil-bearing capacity of micropores within the shell

The fluorescence thin-section images demonstrate that a significant amount of bitumen is present within the pores of the shell, all exhibiting a white-blue fluorescent color (Fig. 7). The distribution pattern of these species correlates with the observed distribution of micropores within the shell (Fig. 7). The pores containing hydrocarbons primarily extend along the long axis of the shell (Fig. 4) but exhibit a notably uneven zonation along the short axis (Fig. 7).

5. Discussion

5.1. Origin of micropores within the shell

5.1.1. Biological origin and depositional environment of the fossilized shells

Morphological characteristics observed in core samples and CT scans indicate that the biological shells in the Early
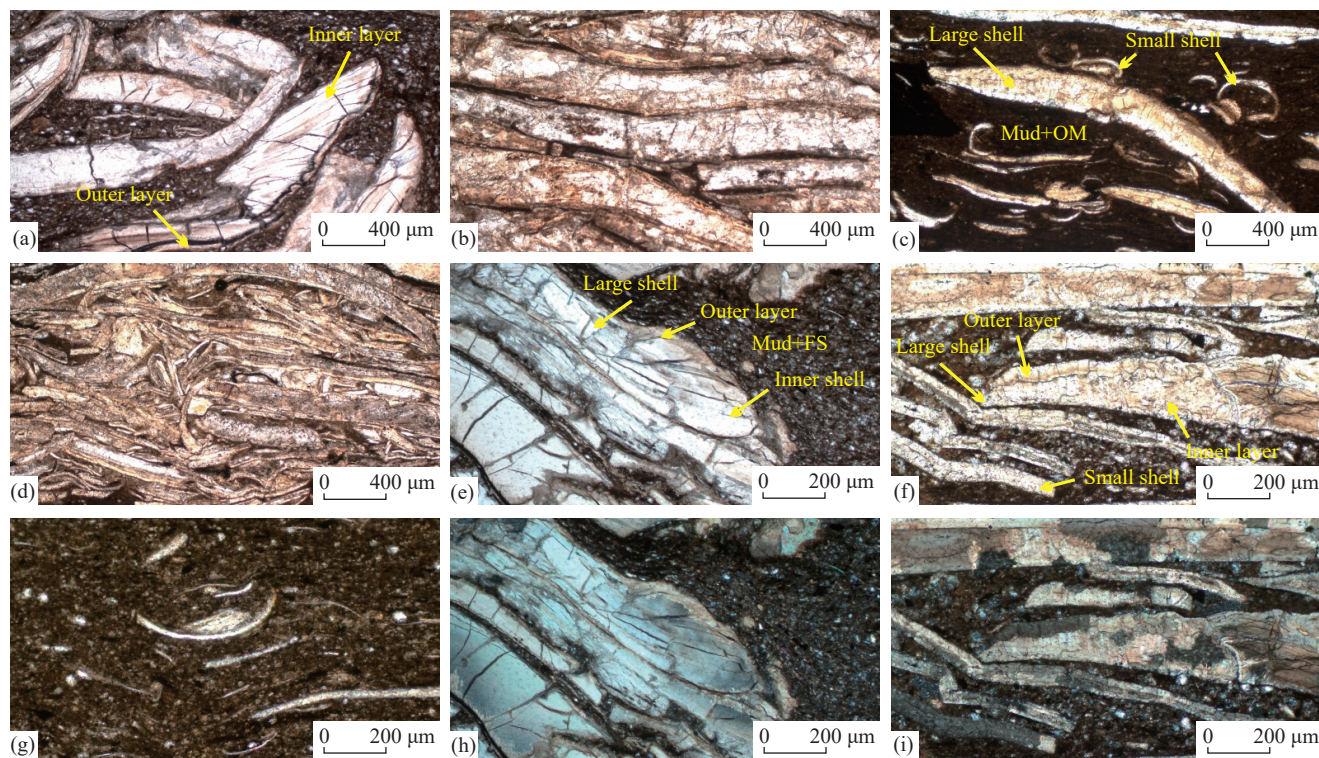
Fig. 3. Thin section images showing the characteristics of shell fossils in bioclastic layers of the Da'anzhai shale, Sichuan Basin. (a) Large shell embedded in shale with inner and outer layer indicated; plane polarized light, D1-3162.8 m. (b) Layer composed almost totally of large shells; plane polarized light, DY-3363.7 m. (c) Large and small shells embedded in shale; plane polarized light, D1-3364.9 m. (d) Layer composed of both large and small shells; plane polarized light, DY-3364.9 m. (e) Large shell, plane polarized light, DY-3162.8 m. (f) Large shell containing relatively pure calcite crystals, plane polarized light; D1-3368.2 m. (g) Small shell embedded in shale; plane polarized light, D1-3162.8 m. (h) Large shell; cross polarized light, D1-3162.8 m. (i) Large shells containing relatively pure calcite crystals; cross polarized light, D1-3368.2 m.
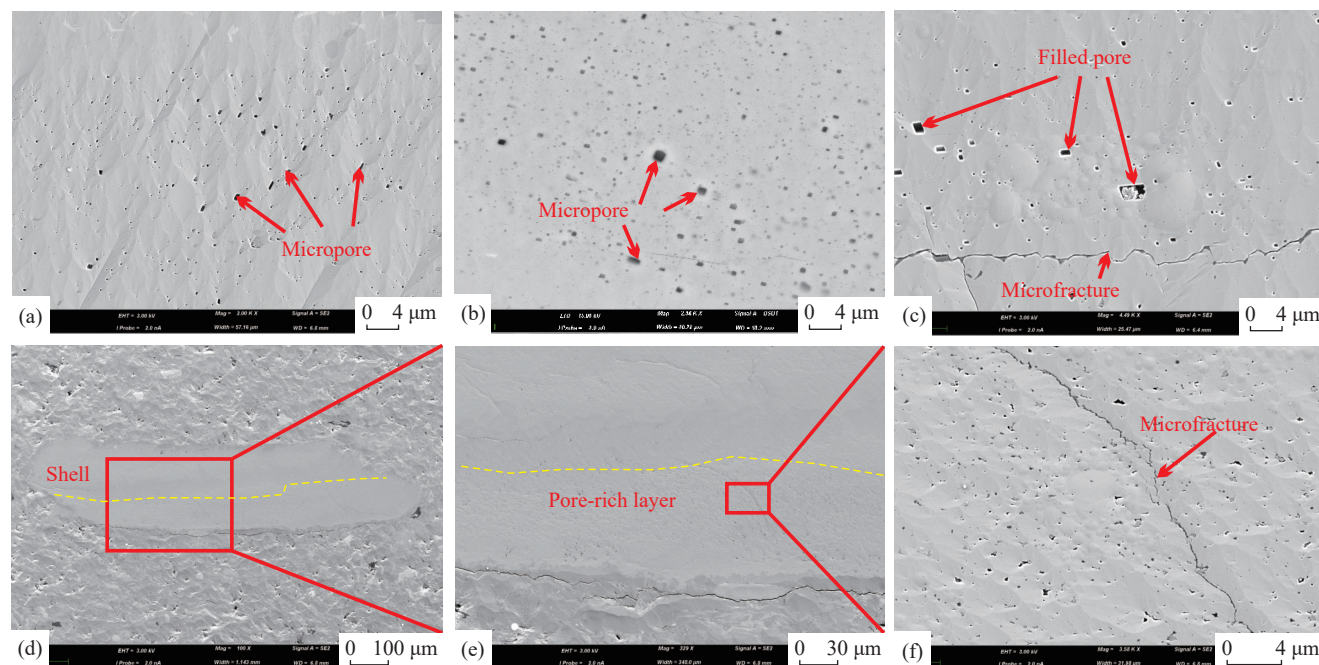
Fig. 4. SEM images showing the micropores within a bivalve shell. (a) Oriented micropores along the shell, PL8, 2570.3 m. (b) Micropores in the pore-rich layer within the shell, D1-3044.5 m. (c) Pseudomorphic crystals filling the pores within a shell, D1- 3044.5 m. (d) Fossil shell in the bioclastic layer, D1-3028.3 m. (e) Boundary of pore-rich layer in a shell, D1-3028.3 m. (f) The microfracture in a shell, D1-3028.3 m.

Jurassic strata of northeastern Sichuan are fossils with the morphological features of bivalve organisms (Fig. 2).

Previous studies have shown that the main carbonate mineral shells in the Early Jurassic strata of southern China originate
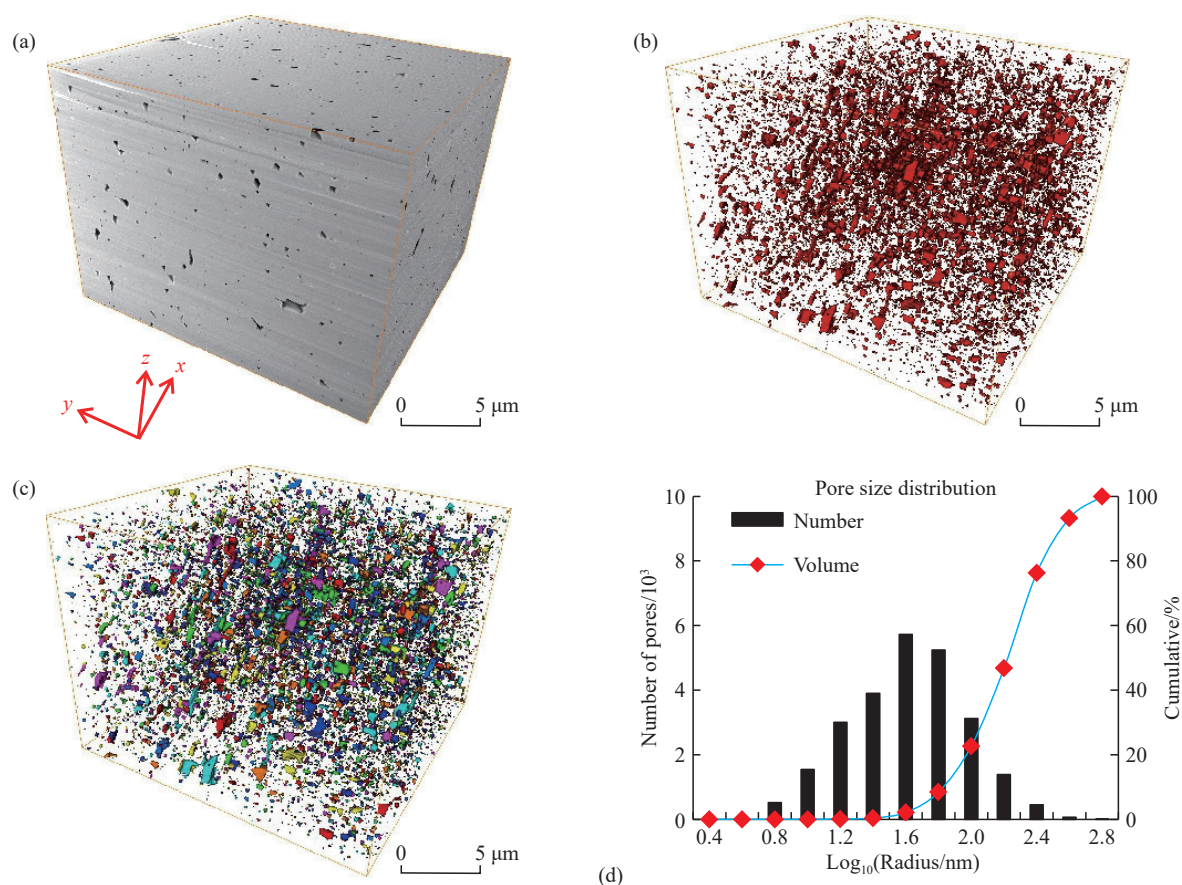
Fig. 5. Three-dimensional reconstruction of the fossil shell layer (PL8, 2570.3 m) from 1500 sequential BSE images by FIB-SEM. (a) Reconstruction of the fossil shell layser from BSE images. (b) Pores within the fossil shell layer. (c) Separated pores shown in different colors within the shell fossil. (d) Pore-size distribution of the pores within the fossil shell layer.

from various bivalve organisms, including the bivalves *Cuneopsis johannisboehmi*, *Psilunio* sp., *Eolamprotula guangyuanensis*, and *Undulatula sichuanensis* (Chen PJ et al., 2006). Bivalves are a diverse group, with most species residing in marine environments, while a minority inhabit freshwater ecosystems (Huang YF et al., 2015). After the Great Extinction at the end of the Permian period, bivalves gradually became the dominant benthic organisms globally, a status they retain to this day (Huang YF et al., 2015).

Bivalve mollusks are benthic organisms that typically inhabit sandy or muddy surfaces at the bottom of water bodies, exhibiting slow and limited mobility (Rindsberg AK, 1994; Uchman A et al., 2011). These organisms primarily acquire nutrients by ingesting sediment from the waterbed, filtering out organic matter, or directly capturing organic debris and microorganisms in the water (Bender K and Davis WR, 1984; Mangano MG et al., 1998).

Bioclastic layers in Early Jurassic shales of northeastern Sichuan are predominantly found in the Da'anzhai section of the Ziliujing Formation and the middle to upper sections of the Lianggaoshan Formation. The Da'anzhai section corresponds the period when the lake level in the region reached its highest point during the Early Jurassic, with the lake's center located in northeastern Sichuan (Fig. 1). During this period large quantities of organic-rich silt layers were deposited, creating favorable conditions for the proliferation

of bivalve benthic organisms (Yang YM et al., 2019; Liu ZB et al., 2020; He WY et al., 2022). During the deposition the Lianggaoshan Formation, the lake basin in northeastern Sichuan had begun to shrink, with the lake becoming shallower and the distribution area and thickness of organic-rich mudstones decreasing (Fig. 1). Thus, although the middle to upper sections of the Lianggaoshan Formation contain the thickest mudstone deposits within the formation, the total abundance of bivalve benthic organisms is still significantly lower than in the Da'anzhai Formation.

5.1.2. The Formation and evolution of micropores in shells

The Bivalvia are a class of mollusks whose shells primarily composed of carbonate minerals (Addadi L et al., 2006). With a large diversity of species, most Bivalvia are marine, while a minority lives in freshwater environments (Huang YF et al., 2015). After the Great Extinction at the end of the Permian period, bivalves gradually became the dominant benthic organisms worldwide, a status they maintain to this day (Huang YF et al., 2015).

The shells of the bivalves are primarily formed by the accretion of mantle epithelial cells, a process that leads to the formation of micropores within the shell (Belcher AM et al., 1996). The bivalve shell can be divided into three parts: the inner mantle epithelial cells, the middle mineral shell, and the outer cuticle (organic epicanium) (Fig. 8).
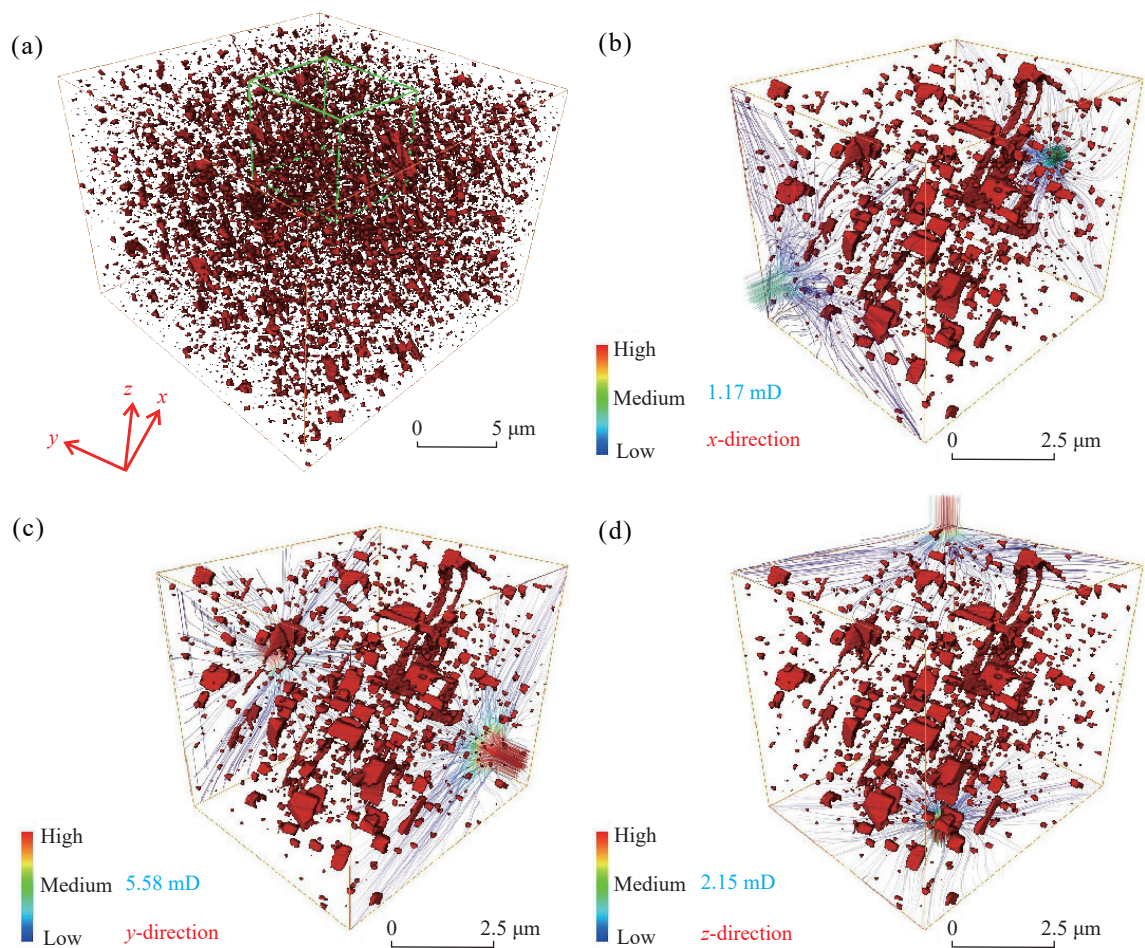
Fig. 6. Simulated 3-dimensional permeability distributions of fossil shell layers, PL8, 2570.3 m. (a) Permeability simulations were performed for the green box in the pore network of the shell layer. (b) Results of permeability simulation of the fossil shell layer in x-direction. (c) y-direction and (d) z-direction.

Table 2. Results of the permeability simulation for the fossil shell shown in Fig. 5 using the Avizo pore network analysis software.

Volume used for permeability simulation /μm³	Resolution/nm	Porosity/%	Direction	Permeability/mD
7.03×5.8×6.17	10×10×10	0.81%	x	1.17
	10×10×10		y	5.58
	10×10×10		z	2.15

During the growth, the outermost cuticle and the inner mantle epithelial cells are formed first. The liquid secreted by the mantle epithelial cells in the small fluid-filled space subsequently forms an outer prismatic shell layer and an inner nacreous shell layer within the cuticle (Munch E et al., 2008; Olson IC et al., 2013). Typically, the outer prismatic shell is made of calcite, while the inner nacreous shell is composed of aragonite (Fig. 8). Both the cuticle and the outer prismatic shell layer are relatively thin, with the inner nacreous shell layer occupying most of the shell's thickness (Fig. 8). The aragonite of the inner shell layer forms multiple small plates, which stack together to create a brick wall structure (Tang ZY et al., 2003; Finnemore A et al., 2012), commonly known as the nacreous structure (Fig. 8).

Boundaries formed between shells developed in different stages constitute "growth lines" that document the shell's growth (Lutz RA, 1976). These growth lines are clearly identifiable in the shell sections of modern bivalves and in the fossils from the northeastern Sichuan region (Fig. 9).

Scanning electron microscopy (SEM) images of modern bivalve mollusk shells reveal a distinct and regular brick-like stacking pattern in the cross-sections of the inner shell layers. This characteristic structure is representative of bivalve mollusk shells (Munch E et al., 2008; Olson IC et al., 2013). Although the fossilized shells from northeastern Sichuan region no longer exhibit discernible brick-like structures, they retain well-defined micropores. These micropores are likely remnants of the original layered structure that survived the cementation and infilling processes during diagenesis, representing a residual framework of fissure networks visible as a pore-rich layer within the shell (Fig. 4).

Within the nacreous layer structure of bivalve organisms, micropores between individual carbonate mineral "bricks" are clearly distinguishable (Munch E et al., 2008; Olson IC et al., 2013) (Fig. 9). These micropores contribute porosity to newly deposited bivalve shells, although this porosity is highly susceptible to infilling during burial and diagenesis in sedimentary environments. Particularly in the vicinity of
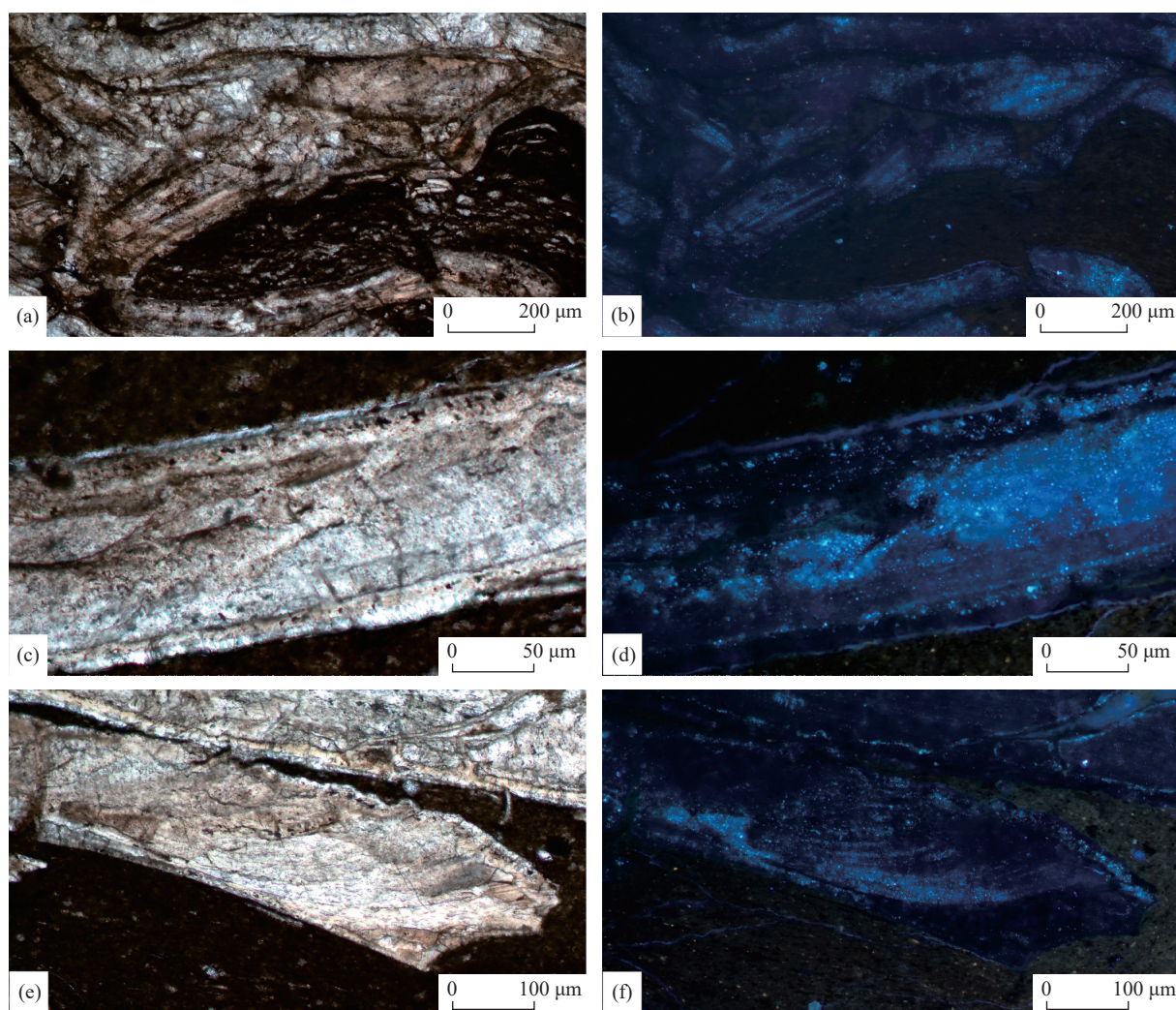
Fig. 7. Images showing the large shells and the liquid hydrocarbons inside under plane-polarized light (left) and reflected fluorescence (right). (a) Deformed large shell, D1, 3363.7 m. (b) Hydrocarbons appear in white-blue fluorescence under ultraviolet light within the deformed shell, D1, 3363.7 m. (c) Individual large shell, D1, 3364.9 m. (d) Hydrocarbons within the micropores exhibiting bright blue fluorescence under ultraviolet light along the long axis of the shell, D1-3364.9 m. (e) Large shell, D1, 3364.9 m. (f) Hydrocarbon filling arranged in ribbons along the short axis of the shell, showing bright blue fluorescence under ultraviolet light, D1, 3364.9 m.

shales, the calcium ions expelled during shale compaction can rapidly cement fractures within these bivalve shells, effectively sealing them. However, due to this proximity to shale, hydrocarbons generated by the shale, particularly mobile light hydrocarbons, can also readily enter these shell micropores. Once these light hydrocarbons enter the pores, the cementation process halts. Consequently, the microporosity observed within the fossil shells is primarily residual porosity preserved due to infusion of hydrocarbons while the fractures in the nacreous layer underwent cementation (Fig. 7). The cementation of carbonate minerals is a diagenetic process that begins in the early stages of rock formation, or even during the penecontemporaneous period, particularly in strata adjacent to shale, where extensive pore-filling by carbonate minerals is frequently observed (Zhong DK et al., 2013; Wang YC et al., 2017; Shang FK et al., 2020; Wang YT et al., 2021; Yu JW et al., 2023). Such filling generally precedes the onset of oil generation in adjacent shale layers. As a result, the liquid hydrocarbons within the shells should not have existed

prior to the formation of micropores. If the relatively abundant pores within the shell remained uncemented after shell formation until the injection of liquid hydrocarbons, these hydrocarbons would have inhibited cementation within the shell, leading to the preservation of a greater number of pores than currently observed. Given that the Lianggaoshan Formation and the Da'anzhai Member are consist of fine-grained and dense shale and siltstone deposits, they do not easily support the migration and injection of hydrocarbons from more distant sources into these shell beds.

5.2. The petroleum geological significance of micropores in carbonate shells

Although the carbonate-based shells are biologically formed biological processes, they are inherently inorganic and incapable of hydrocarbon generating. Therefore, the hydrocarbons they contain are primarily sourced from adjacent hydrocarbon source rocks. As bioclastic carbonate layers often lie adjacent to high-quality source rocks, liquid
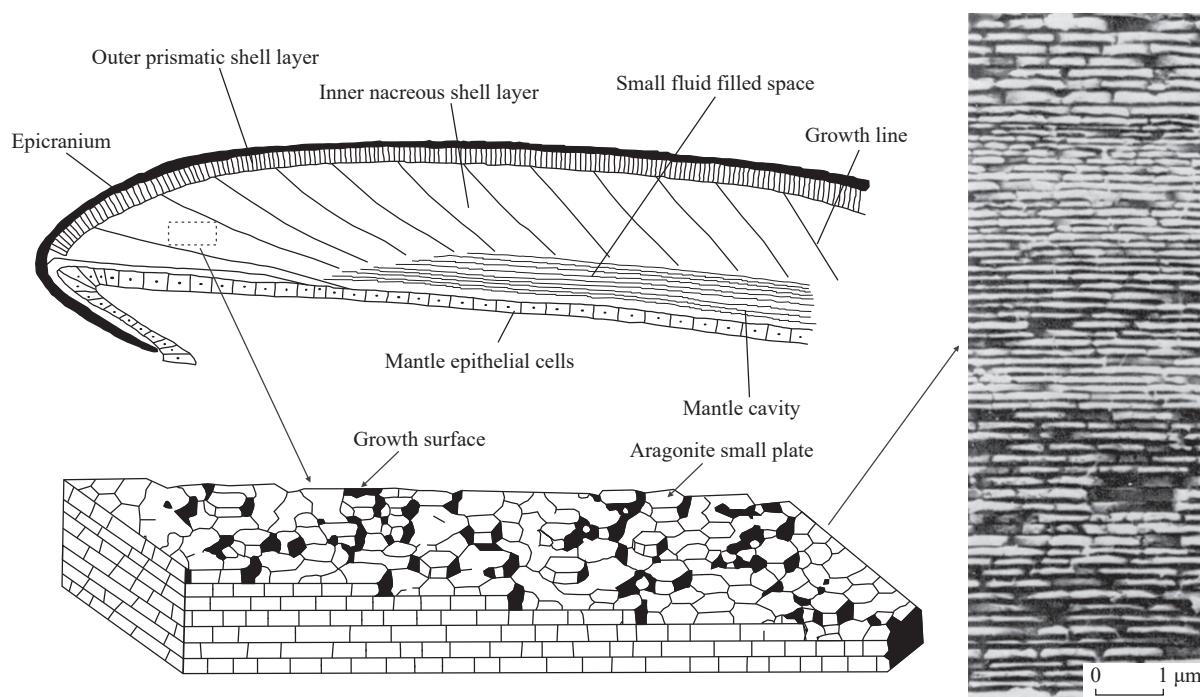
Fig. 8. Typical shell structure of bivalvia and SEM image of the section of inner nacreous shell layer of a modern sample (Lutz RA, 1976; Zhang GS and Xie XD, 2000).
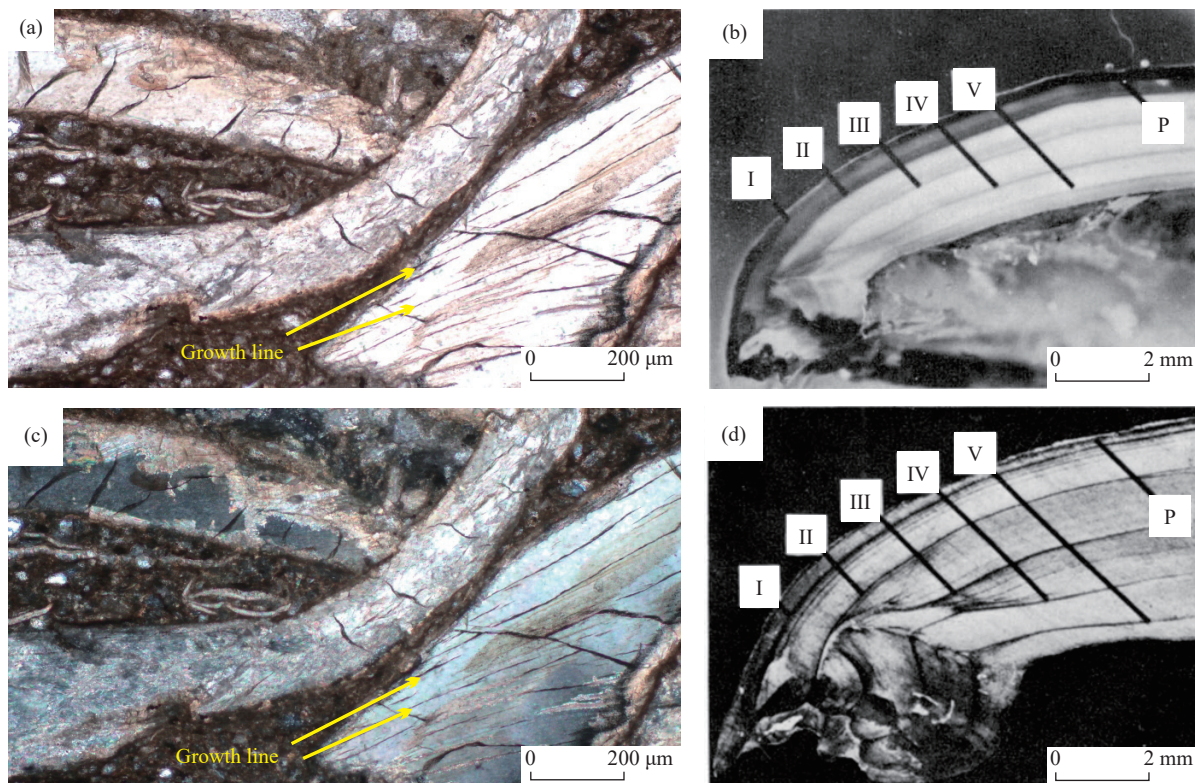

Fig. 9. Comparison of growth lines of Jurassic and modern shells. (a) Large shell with growth line, plane polarized light, DY1-3162.8 m. (b) Modern specimen sampled 29 November 1972 from Damariscotta River shore population (Lutz RA, 1976). (c) Large shell with growth line, cross polarized light, DY1-3162.8 m. (d) Acetate peel of umbonal region of (b) (Lutz RA, 1976).

hydrocarbons or natural gas readily infiltrate the micropores within these biological shells. These pores are typically micropores, less than 250 nm (Fig. 5), which only highly mobile, low molecular-weight hydrocarbons can penetrate

(Badre S et al., 2006). This is evidenced by the uniform blue-white fluorescence observed in the hydrocarbons trapped within the shell micropores, indicating a consistent source and a predominance of highly mature condensate oil (Fig. 7). Due

to the nacreous structure, the shell preserves a significant portionof the original pore and fracture system during sedimentation (Fig. 10). However, under the influence of diagenesis, these reticulate pores and fractures gradually become filled and modified, resulting in a significant reduction in the number of pores and fractures (Fig. 10). Nonetheless, the residual pore and fracture system retains original reticulate structure and its anisotropic permeability (Fig. 6). With increasing burial depth, the organic matter surrounding or adjacent to these shell layers starts generating hydrocarbons (Fig. 10). The lighter hydrocarbon components readily enter these micropores and accumulate within the shell.

Microscopic analysis reveals that the micropores within the carbonate rock shells typically extend in layered zones along the long axis. This leads to a significant increase in fluid permeability along this direction, indicating that these oriented shells exhibit pronounced directional permeability along their long axis. As most shells typically stack in layered formations after deposition, the internally oriented micropores and fractures between different shells may enhance the lateral migration of hydrocarbons within the bioclastic layers.

6. Conclusion

The abundant micro-pores within fossil shells serve as vital storage spaces for hydrocarbons generated in adjacent shales. Most micropores in fossil shells have radii ranging from 100 to 1000 nm, and are uniformly distributed in a grid-like pattern. With an overall porosity of approximately 0.8%, these micropores can effectively store liquid hydrocarbons. Bivalves have been the most widely distributed mollusks since the Mesozoic era. Their benthic habitat often occurs in proximity to organic-rich shales, facilitating the storage of lighter liquid or gaseous hydrocarbons within the micropores of their fossilized shells. The micropores in the shells originate from the brick-stacked nacreous layer, which constitutes the primary component of the bivalve shell. The nacreous layer has a grid-like system of fine pores and cracks. Although these pores and cracks are predominantly filled by diagenesis after sedimentation, the residual micropores still have a significant oil and gas storage capacity and exhibit directional permeability. This suggests that the bioclastic shell layers in mudstones and shales are excellent oil and gas reservoirs and effective migration pathways adjacent to shale intervals, making them promising exploration targets.

CRediT authorship contribution statement

Yong Ma contributed to the manuscript writing, review, and editing. Cheng-yu Yang was responsible for methodology, investigation, review, and editing. Da-hua Li,
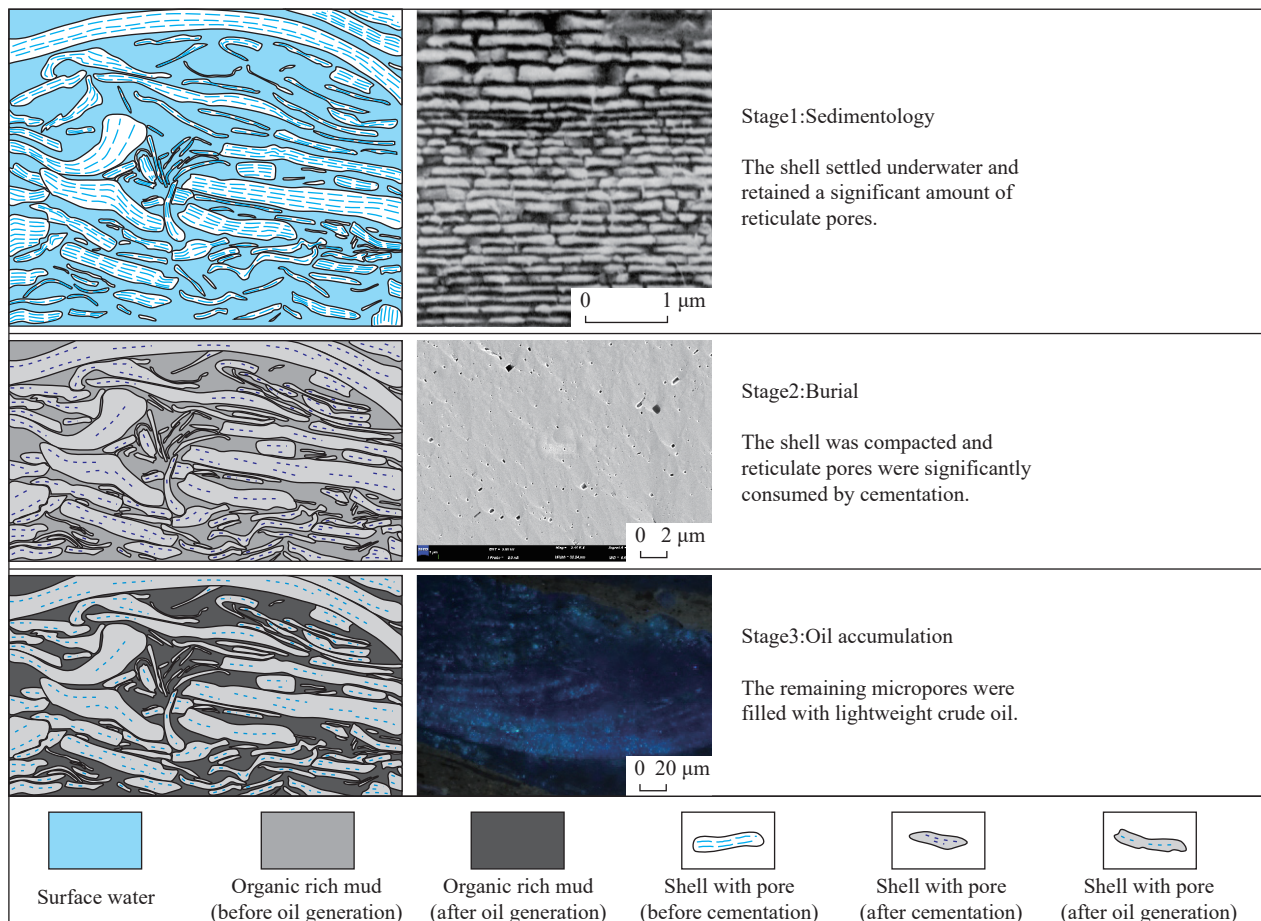

Fig. 10. Schematic diagram showing the concept of the filling of shell fossils in the Jurassic bioclastic layers in the northeastern Sichuan Basin. The evolution of shell fossils modified after Lutz RA (1976).

References

Addadi L, Joester D, Nudelman F, Weiner S. 2006. Mollusk shell formation: a source of new concepts for understanding biomineralization processes. Chemistry, 12(4), 980–987. doi: 10.1002/chem.200500980.

Badre S, Carla GC, Noringa K, Gustavson G, Mullins OC. 2006. Molecular size and weight of asphaltene and asphaltene solubility fractions from coals, crude oils and bitumen. Fuel, 85(1), 1–11. doi: 10.1016/j.fuel.2005.05.021.

Belcher AM, Wu XH, Christensen RJ, Hansma PK, Stucky GD, Morse DE. 1996. Control of crystal phase switching and orientation by soluble mollusc-shell proteins. Nature, 381, 56–58. doi: 10.1038/381056a0.

Bender K, Davis WR. 1984. The effect of feeding by *Yoldia limatula* on bioturbation. Ophelia, 23(1), 91–100. doi: 10.1080/00785236.1984.10426606.

Callow B, Falcon-Suarez I, Ahmed S, Matter J. 2018. Assessing the carbon sequestration potential of basalt using X-ray micro-CT and rock mechanics. International Journal of Greenhouse Gas Control, 70, 146–156. doi: 10.1016/j.ijggc.2017.12.008.

Callow B, Falcon-Suarez I, Marin-Moreno H, Bull JM, Ahmed S. 2020. Optimal X-ray micro-CT image based methods for porosity and permeability quantification in heterogeneous sandstones. Geophysical Journal International, 223(2), 1210–1229. doi: 10.1093/gji/ggaa321.

Cao YC, Xi KL, Niu XB, Lin MR, Ma WJ, Zhang ZH, Hellevang H. 2024. Lamina-scale diagenetic mass transfer in lacustrine organic-rich shales and impacts on shale oil reservoir formation. AAPG Bulletin, 108(7), 1327–1356. doi: 10.1306/12212323018.

Chen PJ, Li JJ, Matsukawa M, Zhang HC, Wang QF, Lockley MG. 2006. Geological ages of dinosaur-track-bearing formations in China. Cretaceous Research, 27(1), 22–32. doi: 10.1016/j.cretres.2005.10.008.

Curtis JB. 2002. Fractured shale-gas systems. AAPG Bulletin, 86(11), 1921–1938. doi: 10.1306/61eeddbe-173e-11d7-8645000102c1865d.

Finnemore A, Cunha P, Shean T, Vignolini S, Guldin S, Oyen M, Steiner U. 2012. Biomimetic layer-by-layer assembly of artificial nacre. Nature Communications, 3, 966. doi: 10.1038/ncomms1970.

Ghanizadeh A, Clarkson CR, Clarke KM, Yang ZR, Rashidi B, Vahedian A, Song CY, DeBuhr C, Haghshenas B, Ardakani OH, Sanei H, Royer DP. 2020. Effects of entrained hydrocarbon and organic-matter components on reservoir quality of organic-rich shales: Implications for "sweet spot" identification and enhanced-oil-recovery applications in the duvernay formation (Canada). SPE Journal, 25(3), 1351–1376. doi: 10.2118/189787-pa.

He WY, Bai XF, Meng QA, Li JH, Zhang DZ, Wang YZ. 2022. Accumulation geological characteristics and major discoveries of lacustrine shale oil in Sichuan Basin. Acta Petrolei Sinica, 43(7), 885–898 (in Chinese with English abstract). doi: 10.7623/syxb202207001.

Horsfield B, Schulz HM, Bernard S, Mahlstedt N, Han YJ, Kuske S. 2020. Oil and gas shales. Hydrocarbons, Oils and Lipids: Diversity, Origin, Chemistry and Fate. Cham: Springer International Publishing, 523–556. doi: 10.1007/978-3-319-90569-3_18.

Huang YF, Tong JN, Xiang Y, Xiao CT, Song HJ, Tian L, Song T, Chu DL. 2015. The extinction and delayed recovery of bivalves during the Permian-Triassic crisis. Earth Science, 40(2), 334–345 (in Chinese with English abstract).

Jarvie DM. 2012. Shale resource systems for oil and gas: Part 2—Shale-oil resource systems. AAPG Memoir, 97, 89–119. doi: 10.1306/13321447m973489.

Ji WM, Hao F, Gong FH, Zhang J, Bai YF, Liang C, Tian JQ. 2024. Petroleum migration and accumulation in a shale oil system of the Upper Cretaceous Qingshankou Formation in the Songliao Basin, northeastern China. AAPG Bulletin, 108(8), 1611–1648. doi: 10.1306/03212423016.

Jin ZJ. 2023. Hydrocarbon accumulation and resources evaluation: Recent advances and current challenges. Advances in Geo-Energy Research, 8(1), 1–4. doi: 10.46690/ager.2023.04.01.

Katz B, Lin F. 2014. Lacustrine basin unconventional resource plays: Key differences. Marine and Petroleum Geology, 56, 255–265. doi: 10.1016/j.marpetgeo.2014.02.013.

Liu ZB, Liu GX, Hu ZQ, Feng DJ, Zhu T, Bian RK, Jiang T, Jin ZG. 2020. Lithofacies types and assemblage features of continental shale strata and their implications for shale gas exploration: A case study of the Middle and Lower Jurassic strata in the Sichuan Basin. Natural Gas Industry B, 7(4), 358–369. doi: 10.1016/j.ngib.2019.12.004.

Loucks RG, Reed RM, Ruppel SC, Hammes U. 2012. Spectrum of pore types and networks in mudrocks and a descriptive classification for matrix-related mudrock pores. AAPG Bulletin, 96(6), 1071–1098. doi: 10.1306/08171111061.

Lutz RA. 1976. Annual growth patterns in the inner shell layer of *Mytilus edulis* L. Journal of the Marine Biological Association of the United Kingdom, 56(3), 723–731. doi: 10.1017/s0025315400020750.

Ma Y, Ardakani OH, Zhong NN, Liu HL, Huang HP, Larter S, Zhang C. 2020. Possible pore structure deformation effects on the shale gas enrichment: An example from the Lower Cambrian shales of the Eastern Upper Yangtze Platform, South China. International Journal of Coal Geology, 217, 103349. doi: 10.1016/j.coal.2019.103349.

Mangano MG, Buatois LA, West RR, Maples CG. 1998. Contrasting behavioral and feeding strategies recorded by tidal-flat bivalve trace fossils from the upper Carboniferous of eastern Kansas. Palaios, 13(4), 335. doi: 10.2307/3515322.

Munch E, Launey ME, Alsem DH, Saiz E, Tomsia AP, Ritchie RO. 2008. Tough, bio-inspired hybrid materials. Science, 322(5907), 1516–1520. doi: 10.1126/science.1164865.

Ni C, Hao Y, Hou GF, Gu MF, Zhang LT. 2012. Cognition and significance of Lower Jurassic daanzhai organic muddy shell limestone reservoir in central Sichuan basin. Marine Origin Petroleum Geology, 17(2), 45–56 (in Chinese with English abstract). doi: 10.3969/j.issn.1672-9854.2012.02.007.

Olson IC, Blonsky AZ, Tamura N, Kunz M, Pokroy B, Romao CP, White MA, Gilbert PUPA. 2013. Crystal nucleation and near-epitaxial growth in nacre. Journal of Structural Biology, 184(3), 454–463. doi: 10.1016/j.jsb.2013.10.002.

Peng S, Marone F, Dultz S. 2014. Resolution effect in X-ray microcomputed tomography imaging and small pore's contribution to permeability for a Berea sandstone. Journal of Hydrology, 510, 403–411. doi: 10.1016/j.jhydrol.2013.12.028.

Pepper A, Perry S, Heister L. 2019. Saturation Isn't What It Used to Be: Towards More Realistic Petroleum Fluid Saturations and Produced Fluid Compositions in Organic-Rich Unconventional ReservoirsProceedings of the 7th Unconventional Resources Technology Conference. July 22-24, 2019. Denver, Colorado, USA. American Association of Petroleum Geologists, 2985–3000. doi: 10.15530/urtec-2019-196.

Raji M, Gröcke DR, Greenwell HC, Gluyas JG, Cornford C. 2015. The effect of interbedding on shale reservoir properties. Marine and Petroleum Geology, 67, 154–169. doi: 10.1016/j.marpetgeo.2015.04.015.

Rindsberg AK. 1994. Ichnology of the Upper Mississippian Hartselle Sandstone of Alabama, with notes on other Carboniferous formations. Geological Survey of Alabama Bulletin, 158, 1−107.

Romero-Sarmiento MF. 2019. A quick analytical approach to estimate both free versus sorbed hydrocarbon contents in liquid-rich source rocks. AAPG Bulletin, 103(9), 2031–2043. doi: 10.1306/02151918152.

Shang FK, Zhang KH, Shi HG, Xu YD, Zhang YJ, Chen L. 2020. "Ternary composite" genesis and petroleum geological significance of calcareous barriers in the 1st sand group of Shawan-1 member of Neogene in the Chepaizi bulge of the Junggar Basin. China Petroleum Exploration, 25(1), 112–125 (in Chinese with English abstract).

Tang ZY, Kotov NA, Magonov S, Ozturk B. 2003. Nanostructured artificial nacre. Nature Materials, 2(6), 413–418. doi: 10.1038/nmat906.

Tiwari P, Deo M, Lin CL, Miller JD. 2013. Characterization of oil shale pore structure before and after pyrolysis by using X-ray micro CT. Fuel, 107, 547–554. doi: 10.1016/j.fuel.2013.01.006.

Uchman A, Mikuláš R, Rindsberg AK. 2011. Mollusc trace fossils Ptychoplasma Fenton and Fenton, 1937 and Oravaichnium Plička and Uhrová, 1990: Their type material and ichnospecies. Geobios, 44(4), 387–397. doi: 10.1016/j.geobios.2010.08.001.

Wang XN, Li JR, Jiang WQ, Zhang H, Feng YL, Yang Z. 2022. Characteristics, current exploration practices, and prospects of continental shale oil in China. Advances in Geo-Energy Research, 6(6), 454–459. doi: 10.46690/ager.2022.06.02.

Wang YC, Hu R, Chen Q, Huang X, Xiao X. 2017. Distribution characteristics and genesis analysis of Cretaceous calcareous sandstone interlayer in Chun17 well area of Chunguang Oilfield. Petroleum Geology and Engineering, 31(5), 44–46 (in Chinese). doi: 10.3969/j.issn.1673-8217.2017.05.012.

Wang YT, Sun GQ, Zhang SC, Chen B, Zhu WJ, Jiang Y. 2021. Characteristics and genesis of carbonate cement in abdomen sandstone in northern margin of Qaidam Basin. Natural Gas Geoscience, 32(7), 1037–1046 (in Chinese with English abstract). doi: 10.11764/j.issn.1672-1926.2021.01.008.

Yang YM, Huang D, Yang G, Li YC, Dai HM, Bai R. 2019. Geological conditions to form lacustrine facies shale oil and gas of Jurassic Daanzhai Member in Sichuan Basin and exploration directions. Natural Gas Exploration and Development, 42(2), 1–12 (in Chinese with English abstract). doi: 10.12055/gaskk.issn.1673-3177.2019.02.001.

Yu JW, Ding W, Zhang X, Qi LQ, Huang SY, Zhang ZY, Zhang YL. 2023. Genesis of carbonate cement and influence on reservoir quality of the badaowan formation in AH5 well block of Junggar basin. Geoscience, 37(5), 1336–1344 (in Chinese with English abstract). doi: 10.19657/j.geoscience.1000-8527.2023.035.

Yuan SY, Lei ZD, Li JS, Yao ZW, Li BH, Wang R, Liu YS, Wang QZ. 2023. Key theoretical and technical issues and countermeasures for effective development of Gulong shale oil, Daqing Oilfield, NE China. Petroleum Exploration and Development, 50(3), 638–650. doi: 10.1016/S1876-3804(23)60416-1.

Zhang GS, Xie XD. 2000. Ultrastructure and formation theory of nacre shells. Journal of Mineralogy and Petrology, 20(1), 11–16 (in Chinese with English abstract). doi: 10.19719/j.cnki.1001-6872.2000.01.003.

Zhong DK, Zhu HH, Sun HT, Cai C, Yao JL, Liu XY, Deng XQ, Luo AX. 2013. Diagenesis and porosity evolution of sandstones in Longdong area, Ordos basin. Earth Science Frontiers, 20(2), 61–68 (in Chinese with English abstract).

Zhu HH, Chen L, Cao ZL, Wang ML, Hong HT, Li YC, Zhang R, Zhang SM, Zhu GY, Zeng X, Yang W. 2022. Microscopic pore characteristics and controlling factors of black shale in the Da'anzhai Member of Jurassic Ziliujing Formation, central Sichuan Basin. Oil & Gas Geology, 43(5), 1115–1126 (in Chinese with English abstract). doi: 10.11743/ogg20220509.